

The largest Kuiper belt objects

Michael E. Brown

California Institute of Technology

ABSTRACT

While for the first decade of the study of the Kuiper belt, a gap existed between the sizes of the relatively small and faint Kuiper belt objects (KBOs) that were being studied and the largest known KBO, Pluto, recent years have seen that gap filled and the maximum size even expanded. These large KBOs occupy all dynamical classes of the Kuiper belt with the exception of the cold classical population, and one large object, Sedna, is the first member of a new more distant population beyond the Kuiper belt. Like Pluto, most of the large KBOs are sufficiently bright for detailed physical study, and, like Pluto, most of the large KBOs have unique dynamical and physical histories that can be gleaned from these observations. The four largest known KBOs contain surfaces dominated in methane, but the details of the surface characteristics differ on each body. One large KBO is the parent body of a giant impact which has strewn multiple fragments throughout the Kuiper belt. The large KBOs have a significantly larger satellite fraction than the remainder of the Kuiper belt, including the only known multiple satellite systems and the relatively smallest satellites known. Based on the completeness of the current surveys, it appears that ~ 3 more KBOs of the same size range likely still await discovery, but that tens to hundreds more exist in the more distant region where Sedna currently resides.

1. Introduction

While once Pluto appeared as a unique object in the far reaches of the solar system, the discovery of the Kuiper belt caused the immediate realization that Pluto is a member of a much larger population. But while Pluto's orbit makes it a typical member of Kuiper belt population dynamically, Pluto itself has still remained special as one of the few trans-Neptunian objects bright enough for detailed studies. Much of what we understand of the composition, density, and history of objects in the Kuiper belt ultimately derives from detailed studies of Pluto.

Recently, however, surveys of the Kuiper belt began to discover Kuiper belt objects (KBOs) of comparable and now even larger size than Pluto. The largest survey to date has used the 48-inch Palomar Schmidt telescope to cover almost 20,000

square degrees of sky to a limiting magnitude of $R \sim 20.5$ (Figure 1). This survey has uncovered most of the known large KBOs (i.e. Trujillo and Brown 2003; Brown et al. 2004, 2005*b*). A total of 71 objects beyond 30 AU have been detected, of which 21 were previously known (or have been independently discovered subsequently). Recovery of objects is still underway to define the dynamics of the large objects; to date 54 of the 71 objects have secure orbits.

This survey for the largest Kuiper belt objects serves both as a search for individual objects bright enough for detailed study and also as the first modern wide-field survey of the outer solar system to more fully define the dynamical properties of the entire region. In this chapter we will first survey the dynamical properties of the largest KBOs and compare them to the population as a whole, then we will examine the largest individual

KBOs, and finally we will review the bulk properties of these largest objects, summarized in Table 1.

2. Population properties of the largest KBOs

2.1. Dynamical distribution

As first noticed by Levison and Stern (2001), KBOs brighter than an absolute magnitude of about 6.0 are distributed with a much broader inclination distribution than those fainter. Physically this trend is better stated that the low inclination population is missing the largest objects (or at least the brightest objects) that are found in the high inclination population. This effect is easily visible in a simple plot of inclination versus absolute magnitude, but such a direct comparison of simple discovery statistics is thoroughly biased by the fact that most surveys for fainter KBOs have been restricted much more closely to the ecliptic and thus preferentially find low inclination objects.

One method for examining a population relatively unbiased by differences in latitudinal coverage of surveys is to consider only objects detected at a restricted range of latitudes. In such debiased examinations, no statistically significant difference can be discerned between the size distribution of the high and low inclination populations. From the discovery statistics alone no definitive indication exists that the populations differ. The question must be addressed with actual measurements of sky densities of KBOs of different brightnesses rather than simple discovery statistics.

Fortunately, the Palomar survey for large KBOs is complete for low inclinations (with the exception of the galactic plane), so we now know that there are *no* objects brighter than absolute magnitude 4.5 in the low inclination population (or, more pertinently, in the cold classical region of the Kuiper belt, defined by Morbidelli and Brown (2005) as the dynamically and physically distinct subpopulation of classical KBOs with uniquely uniform red colors and inclinations lower than about 4 degrees), while in the excited population (defined as the resonant, scattered, and hot classical population) 29 objects brighter than that absolute magnitude are currently known to exist, with the current brightest (Eris) known having an absolute

magnitude of -1.2. The difference in maximum brightness and presumably maximum size between the cold classical and the excited populations is vast.

This difference in maximum size places a powerful constraint on the dynamical rearrangement of the outer solar system. No dynamical process can preferentially damp the inclinations of only the small KBOs nor preferentially excite the inclinations of only large KBOs, so the high and low inclination populations must have either formed at different times or in different places. A current working hypothesis for the larger sizes of the high inclination population was suggested by Levison and Stern (2001) and examined in detail by Gomes (2003). They noted that the difference in size distribution can be explained if the largest objects formed in the solar nebula closer to the sun where nebular densities were higher and growth times were faster and that the objects closer to the sun suffered more extreme scattering by Neptune and thus acquired higher inclinations. Other forces may be at play, however, and a fully convincing explanation remains elusive.

A survey of the largest Kuiper belt objects, then, is only a survey of the excited populations of the Kuiper belt. With this caveat, we can now examine the spatial distribution of the largest Kuiper belt objects. Figure 2 shows the latitudinal distribution, corrected for coverage completeness, of the KBOs from our survey. The prominent peaks around 10 degrees north and south ecliptic latitude cannot be modeled with any simple inclination distribution of objects in circular orbits. Even if all objects in the sky had inclinations of 10 degrees or higher, more objects would appear at lower latitudes than are seen in the survey. While such a latitudinal distribution is impossible for objects with circular or even randomly oriented orbits, many of the objects are consistent with being resonant objects and thus can have preferential orientations in the sky. Pluto, for example, as well as many other KBOs in 3:2 resonance with Neptune, comes to perihelion near its maximum excursion above the ecliptic. This effect will cause a magnitude-limited survey to preferentially detect resonant objects at large distances above the ecliptic. A full examination of this effect awaits full dynamical characterization of the survey population, but from the preliminary data it appears

that resonances are likely able to explain these high latitude concentrations. If true, the high latitude concentrations are not likely a characteristic of the largest KBOs, but a general property of the high inclination Kuiper belt which has not been adequately surveyed until now. The resonant population may be significantly more populated than low latitude surveys have indicated.

2.2. Beyond the Kuiper belt

Among the large objects detected, one appears dynamically distinct from the entire Kuiper belt population. Sedna has a perihelion well beyond the main concentration of KBOs and an extreme eccentric orbit with a aphelion around 900 AU (Brown et al. 2004). Though the discovery of Sedna presages a large population in this distant region beyond the Kuiper belt, no surveys for fainter objects have yet succeeded in detecting such distant objects. While some bias against the slow motions of these objects presumably exists in the main KBO surveys, it is also possible that Sedna has an albedo higher than the more numerous smaller members of the population. Sedna could be thus, like Pluto, an atypically bright member of its population which allows us to detect it much more easily than would have been otherwise possible.

Sedna exists in a dynamical region of the solar system that was not expected to be occupied. It has been proposed to be part of a fossilized inner Oort cloud (Brown et al. 2004; Brassier et al. 2006), a product of a single anomalous stellar encounter (Morbidelli and Levison 2004), an object captured from a passing star (Kenyon and Bromley 2004), a consequence of scattering by now ejected Kuiper belt planets (Gladman and Chan 2006), a signature of perturbation by a distant massive planet (Gomes et al. 2006) and others. Each of these processes creates a dynamically unique population in this region beyond the Kuiper belt. Finding even a handful more of these distant objects should give powerful insights into some of the earliest processes operating at the beginning of the solar system.

This distant population could be significantly more massive than that of the Kuiper belt. Sedna is currently near perihelion of its 11,000 yr orbit. It would have been detected in the Palomar survey only during a ~ 150 year period surrounding peri-

helion, suggesting that the total number of Sedna-sized or larger objects in the distant population is between about 40 and 120. The total number of Sedna-sized or larger objects in the Kuiper belt is $\sim 5 - 8$. If the distant population has the same size distribution as the Kuiper belt – which seems likely given that the Kuiper belt is the most likely source region for this population – this number of Sedna-sized objects suggests a total mass at least an order of magnitude higher than that in the Kuiper belt.

2.3. Size distribution

A finite discrete population which generally follows a power-law size distribution cannot maintain this distribution at the largest sizes. Early surveys of the Kuiper belt expected that for the brightest objects the number of detections would fall significantly below the power-law prediction. Figure 3 shows the opposite. For objects brighter than $R \sim 19.8$ the power law found by Bernstein et al. (2004) for the excited population falls well short of the actual numbers of detections. This increase in the numbers of bright objects over that expected is a consequence of the general increase in albedo with size occurring for these objects (see chapter by Stansberry et al.). A plot of number of objects versus absolute magnitude shows the same trend (with a bias towards higher absolute magnitude because of the flux-limited nature of the survey), and the location of the deviation from the power law is a useful indicator of the approximate location where albedo changes begin to be important. Eight objects brighter than $H \sim 3$ deviate most strongly from the power law and are a convenient dividing line between the largest individual KBOs and the remaining population. Each of these largest KBOs has interesting unique properties that we describe below.

3. Individual properties of the largest KBOs

3.1. Eris

Eris is currently the largest known object in the Kuiper belt. Direct measurement of the size with the Hubble Space Telescope gives a diameter of 2400 ± 100 km (Brown et al. 2006*a*), while radiometric measurement with IRAM gives 3000 ± 400 (Bertoldi et al. 2006). While the two measure-

ments appear discrepant, they only differ by 1.5σ owing to the large uncertainty in the radiometric measurement. We will take the measurement with the smaller uncertainty for the remainder of the discussion but comment on the larger diameter at the end. This size measurement implies a remarkably high V-band albedo of 0.86 ± 0.07 .

The infrared spectrum of Eris is dominated by absorption from methane similar to the spectrum of Pluto (Brown et al. 2005*b*) (Figure 4). Unlike Pluto, however, the infrared spectrum of Eris shows no evidence for the small shifts in the wavelength of the methane absorption associated with methane being dissolved in a nitrogen matrix. The weakest methane absorptions in the visible, however, do possibly show a small shift (Licandro et al. 2006*a*), perhaps suggesting that methane and nitrogen are layered, with mostly pure nitrogen on the surface (where it is probed by the strong absorption features which show no shifts) and dissolved nitrogen below (where it is probed by the weak absorption features which require long path lengths to appear). The weak $2.15 \mu\text{m}$ absorption feature of nitrogen ice has not been definitively identified, but at the low temperature expected on Eris nitrogen should be in its α , rather than β form as it is on Pluto. The α form has an absorption even weaker than that of the β form (Grundy et al. 1993; Tryka et al. 1995) so detection may be extremely difficult even if nitrogen is indeed abundant.

The visible properties of Eris also differ from those of Pluto. Eris is less red than Pluto, and, while Pluto has one of the highest contrast surfaces in the solar system and varies in brightness by 36% over a single rotation (see Brown 2002), no variation has been seen on Eris to an upper limit of 0.05 magnitudes (Carraro et al. (2006) report a photometric variation on one of five nights of ~ 0.02 magnitudes, but no additional observations have confirmed this potential long-term variability).

The high albedo, lower red coloring, and lack of rotational variation on Eris are all consistent with a surface dominated by seasonal atmospheric cycling. With Eris currently near aphelion at 97 AU the radiative equilibrium temperature is ~ 20 K and nitrogen and methane have essentially zero vapor pressures, compared to vapor pressures of $17 \mu\text{bar}$ and 2nbar at the ~ 36 K equilibrium tem-

perature at the 38 AU perihelion. At the current aphelion position, the perihelion atmosphere should be collapsed onto the surface as $0.6 \mu\text{m}$ of methane and 2mm of nitrogen. The darker and redder regions such as those on Pluto, which give Pluto its strong contrast, red color, and lower average albedo, should be covered, giving Eris a more uniform, brighter, and less red surface. Indeed, the high albedo of Eris appears similar to individual regions on Pluto where no dark material appears to be present (Young et al. 2001). As Eris proceeds from aphelion and the surface warms we should expect that darker regions will become uncovered and the surface will appear darker, redder, and more Pluto-like. While this story for the seasonal evolution of surface of Eris consistently explains many aspects of the observations, the pure methane ice on the surface remains unexplained. Methane will freeze out before nitrogen, so the surface might be expected to be layered with methane below nitrogen, with perhaps a mixed Pluto-like layer from perihelion below, but better constrained observations and more detailed modeling will be required to understand the surface state and evolution.

Eris is orbited by an apparently single satellite, Dysnomia, approximately 250 times fainter than Eris (Brown et al. 2006*b*; Brown and Schaller 2007). More distant satellites up to 10 times fainter than Dysnomia can be ruled out from deep HST observations (Brown and Suer 2007). Models for satellite capture which appear successful at describing many of the large satellites detected around many Kuiper belt objects (Goldreich et al. 2002) cannot account for the presence of such a small satellite. The most likely creation mechanism appears to be impacts such as modeled by Canup (2005) who, while attempting to find models describing the Charon-forming impact, found many cases in which the impact generated a disk which could coalesce to form a much smaller satellite. The near circular orbit of Dysnomia ($e < 0.017$) is also consistent with the idea of formation from a disk and outward tidal evolution.

From the orbit of Dysnomia, the mass of Eris is found to be $(1.66 \pm 0.02) \times 10^{22} \text{kg}$ or $27 \pm 2\%$ greater than that of Pluto (Brown and Schaller 2007). Using the HST size measurement the density is then $2.3 \pm 0.3 \text{g cm}^{-3}$, with almost all of the uncertainty due to the uncertainty in the size mea-

surement. The density is consistent on the lower end with the $2.03 \pm 0.06 \text{ g cm}^{-3}$ density of Pluto and on the high end with the $\sim 2.6 \text{ g cm}^{-3}$ density of 2003 EL61 (see below). Note that the larger size measurement from IRAM would give a density of $1.1 \pm 0.6 \text{ g cm}^{-3}$, which, when comparing to other large KBOs and icy satellites, appears unreasonably low for an object of this size (see below).

We might expect that the disk forming impact that generated Dysnomia would have removed some ice from Eris, leading to a higher density than that of Pluto. A more accurate measurement of the density, which would require a more accurate measurement of the size, is clearly warranted. It appears that only an occultation is likely to give an improved size estimate for Eris, and, with Eris far from the galactic plane, opportunities will be limited.

3.2. Pluto

Pluto, discussed in detail in the chapter by Stern, is the largest object in the highly populated 3:2 mean motion resonance with Neptune. Its high albedo and current position near perihelion make it the brightest object in the Kuiper belt and thus the first discovered and most heavily observed. Physically, it appears to be a slightly smaller twin of Eris. The main visible differences appear to be the redder color, the presence of dark areas on the surface, and the different state of methane on the surface. As discussed above, most of these differences can be explained as an expected consequence of the closer heliocentric distance of Pluto.

Pluto is surrounded by a system of one large (Charon)(Christy and Harrington 1978) and two small satellites (Nix and Hydra)(Weaver et al. 2006). Modeling by Canup (2005) suggests that the large satellite Charon can be explained as a consequence of a grazing collision between the proto-Pluto and Charon in which little exchange or heating takes place. While no detailed modeling of the formation of the smaller satellites has been performed, their similar orbital plane to Charon and near-circular orbits (Buie et al. 2006) suggest that they were formed in the same collision.

3.3. Sedna

While the size of Sedna remains uncertain, an upper limit can be placed from Spitzer observations (see chapter by Stansberry et al.), and a more tenuous lower limit can be placed by assuming that the geometric albedo at all wavelengths is lower than 100% (which need not necessarily be true). These limits constrain the V albedo of Sedna to be between 0.16 and 0.30 and the diameter to be between 1200 and 1600 km. A deep HST search for satellites has revealed no candidates to a limit of about 500 times fainter than the primary (Brown and Suer 2007).

Sedna is one of the reddest KBOs known, and in moderate signal-to-noise data, the infrared spectrum appears to contain methane and perhaps nitrogen (Barucci et al. 2005)(Figure 4). The visible-to-infrared spectrum and moderate albedo is consistent with an object covered in dark red organic tholins but with some covering of methane and nitrogen frosts. Sedna is currently at 90 AU and 70 years away from its 76 AU perihelion in its 11,000 year orbit which takes it to 900 AU. It is currently warming and developing whatever limited atmosphere it will have. A 76 AU equilibrium temperature atmosphere of $\sim 160 \text{ nbar}$ of nitrogen will correspond to a $\sim 40 \mu\text{m}$ solid layer of nitrogen ice at aphelion and a $\sim 36 \mu\text{m}$ layer at its current position of 90 AU.

The darker and redder surface of Sedna is consistent in albedo and color with the darker regions on Pluto. The long orbital period and high eccentricity mean that Sedna spends very little time near perihelion, so much more time is available for solid state processing of the material than there is for surface regeneration. The extremely low temperature of Sedna prevents much of an atmosphere even near perihelion and thus no extensive frost surface should ever develop.

3.4. 2005 FY9

2005 FY9 is the brightest KBO after Pluto, and radiometric measurements from the Spitzer Space Telescope (see chapter by Stansberry et al.) suggest a diameter of 1500 ± 300 and an albedo of $80^{+10}_{-20}\%$. Like Eris, Pluto, and Sedna, 2005 FY9 has a surface spectrum dominated by methane (Barkume et al. 2005; Licandro et al. 2006*b*; Brown et al. 2007*a*), but the methane ab-

sorption features on 2005 FY9 are significantly deeper and broader than those on the other objects (Fig. 4). The depth and breadth of solid state absorption features is a function of optical path length through the absorbing material, so the features on 2005 FY9 can be interpreted as being due to extremely large (~ 1 cm) methane grains on 2005 FY9, or, likely more appropriately, as due to a slab of methane ice with scattering impurities separated by ~ 1 cm. Methane grain sizes on the other bodies are closer to $100\mu\text{m}$ in contrast.

In addition to the large methane path lengths, 2005 FY9 differs from Pluto in that even moderately high signal-to-noise spectra show no evidence for the presence of the $2.15\ \mu\text{m}$ nitrogen ice absorption feature (Brown et al. 2007a). Nitrogen appears depleted on 2005 FY9 relative to methane by at least an order of magnitude compared to Pluto. Visible spectroscopy shows evidence, however, for slight shifts in the wavelengths of the methane absorptions features which could be indicative of a small amount of surface coverage of methane dissolved inside nitrogen (Tegler et al. 2007).

Finally, 2005 FY9 has a clear signature of the presence of small grains of ethane, in addition to the methane (Brown et al. 2007a). Ethane is one of expected dissociation products of both gaseous and solid-state methane.

All of these unique characteristics of 2005 FY9 can be interpreted as being due to a large depletion of nitrogen on the object. The depletion of nitrogen would make methane the dominant volatile on the surface and allow grains of relatively pure methane to grow large as the grains of nitrogen do on Pluto. In addition, the presence of methane in pure rather than diluted form would allow the solid state degradation of methane to ethane that would not be possible with methane diluted in small concentrations in nitrogen. 2005 FY9 may be a transition between the larger surface volatile-rich objects and the smaller surface volatile-depleted objects.

2005 FY9 is the largest KBO to have no known satellite. Deep observations from HST place an upper limit for the brightness of faint distant satellites of one part in 10000 (Brown and Suer 2007).

3.5. 2003 EL61

2003 EL61 was first found to be unusual due to its rapid rotation and large light curve variation. Rabinowitz et al. (2006) inferred that 2003 EL61 was a rapidly rotating ellipsoid with a 4 hour rotation period. Assuming that the primary spins in the same plane as the first satellite discovered (Brown et al. 2005a), the light curve and period suggest a body with a density of $2.6\ \text{g cm}^{-3}$, a size (based on the density and mass determined from the satellite orbit) of $2000 \times 1500 \times 1000\ \text{km}$, and a visual albedo (based on the derived size and on the brightness) of 0.73 (the formal uncertainties on these parameters are small, but probably do not reflect the true uncertainties in our understanding of the interior state of large icy bodies and the degree to which uniform density hydrostatic equilibrium holds), consistent with infrared spectra showing deep water ice absorption (Trujillo et al. 2007).

Infrared spectroscopy of the satellite revealed the deepest water ice absorption features of any body detected in the outer solar system (Barkume et al. 2006), which effectively ruled out a capture origin, as capture of a spectrally unique body appears implausible. The rapid rotation, high density, unusual satellite spectrum, and the discovery of a second inner satellite (Brown et al. 2006b) all strongly point to a collisional origin for this system.

A large infrared survey showed that a small number of KBOs have deep water ice absorptions similar to that of 2003 EL61 and almost as deep as its satellite (see Figure 4 in chapter by Barucci et al.). Remarkably, these KBOs are all dynamically clustered near the dynamical position of 2003 EL61 itself. Determination of the proper orbital elements of these objects shows that they represent a tight dynamical family separated by only $140\ \text{m s}^{-1}$ (Brown et al. 2007b). Such a tight dynamical clustering is itself unusual enough; coupled with the spectral similarity and the additional evidence for a giant impact, it becomes clear that the objects in this family are the collisional fragments of a giant impact on the proto-2003 EL61. While the fragments themselves are tightly clustered, 2003 EL61 itself has a velocity difference of approximately $500\ \text{m s}^{-1}$ from the fragments. This difference is easily explained by the residence

of 2003 EL61 with the 12:7 mean motion resonance with Neptune which causes long term eccentricity and inclination evolution that can take an object from near the center of the cluster to the position of 2003 EL61 on a time scale of ~ 1 Gyr.

While a giant impact on the proto-2003 EL61 appears capable of explaining each of the individual observations, some mysteries remain. In modeling to date, impacts are seen to either disperse fragments or create a disk out of which satellites can form. 2003 EL61 appears to have done both. In addition, the very small velocity dispersion of the family implies that the fragments left the surface of 2003 EL61 with velocities a small fraction above the 1 km s^{-1} escape velocity. Detailed modeling will be required for a further understanding of the 2003 EL61 system.

3.6. Other large objects

The three other objects in our collection of large KBOs each also have unique properties. Quaoar and Orcus each have water ice absorption among the deepest of non-2003 EL61 fragment KBOs (Jewitt and Luu 2004; de Bergh et al. 2005; Trujillo et al. 2005). Ixion is the largest known object with a nearly featureless infrared spectrum (Brown et al. 2007b).

The infrared spectrum of Quaoar has an absorption feature at $2.2 \mu\text{m}$ that has been interpreted as being due to ammonia (Jewitt and Luu 2004) in analogy to an absorption feature on Charon (Brown and Calvin 2000), though the two spectra appear different. The absorption feature is also, however, consistent with the position of one of the strongest absorptions for methane. More detailed observations to constrain the composition of the surface of Quaoar are clearly warranted. Quaoar is, in addition, the smallest object known to have a faint satellite (fractional brightness of 0.6%) like those of Eris, Pluto, and 2003 EL61 (Brown and Suer 2007).

Orcus is a Plutino with an orbit which is nearly a mirror-image of that of Pluto. It is the largest KBO with an (apparently) single large (fractional brightness of 8%) satellite; deep HST images show that any more distant satellites must be fainter than Orcus by at least a factor of 1000 (Brown and Suer 2007). Outer satellites of the relative faintness of those of Pluto would remain undetected.

The satellite of Orcus is on a near-circular orbit with a 9.5 day period, consistent with outward evolution from an initially tighter orbit.

Ixion is the brightest object in absolute magnitude with a nearly featureless infrared spectrum, though it is not clear that it is the largest such object. Spitzer observations (see chapter by Stansberry et al.) only moderately constrain the size to $590 \pm 190 \text{ km}$ and the albedo to between ~ 9 and 30%. A handful of other KBOs have Spitzer measurements of a similar or greater size, including Varuna, Huya, 2002 AW197, 2002 UX25, 2004 GV9, 2002 MS4 and 2003 AZ84, and their derived albedos range from 6 to 30%. Some of these objects (2002 UX25 and 2003 AZ84) are known to have moderately large close satellites, and one – Varuna – is known to be a rapid rotator with similarities to 2003 EL61 (Jewitt and Sheppard 2002), but, in general, these objects appear to share few of the properties of the unique larger KBOs.

4. Ensemble properties

4.1. Surface composition

The most striking visible difference between the largest KBOs and the remainder of the population is the presence of volatiles such as methane, nitrogen, and CO in the spectra of the large objects compared to relatively featureless spectra of the remaining objects. The transition from small objects with volatile-free to large objects with volatile-rich surfaces appears to be explainable with a simple model of atmospheric escape shown in Figure 5 (Schaller and Brown 2007). Most KBOs are too small and too hot to be able to retain volatiles against atmospheric escape over the life of the solar system, a few objects are so large or so cold that they easily retain volatiles, and a small number are in the potential transition region between volatile free and volatile rich surfaces. 2003 EL61 is sufficiently large that it could retain volatiles, but it seems likely that the giant impact which removed much of its water ice would have removed much of the volatile mass, also, either through direct ejection or heating. 2005 FY9 and Quaoar are both sufficiently hot that the low-vapor-pressure nitrogen should all have escaped, but the lower-vapor-pressure methane could still be retained. This depletion of nitrogen relative to methane is precisely what is observed on 2005

FY9. On Quaoar, if the $2.2 \mu\text{m}$ absorption is interpreted as being due to methane instead of ammonia, it would appear that Quaoar is in the last stages of volatile loss.

The model shown in Figure 5 provides the first basic framework for understanding the surface compositions of the objects in the Kuiper belt. The vast majority of the known objects are too small and/or too hot to have the possibility of retaining any surface volatiles. Surfaces dominated by relatively featureless involatile heavier organics or exposures of water ice (see chapter by Barucci et al.) are therefore expected on such objects. Volatile-rich surfaces are only possible on these largest of the bodies in the Kuiper belt. In the region beyond the Kuiper belt inhabited by bodies such as Sedna, we should expect that most of the bodies – even relatively small ones – will have the capability of retaining surface volatiles.

The largest non-methane objects have the deepest water ice absorption features (ignoring the presumably special case of 2003 EL61 and its fragments), even taking into account the lower signal-to-noise of the spectra of the fainter objects (see Figure 4 of the chapter by Barucci et al.). Unlike for the presence or absence of surface volatiles no clear explanation of this trend is apparent, though a partial explanation could include the initially higher temperatures of the larger objects leading to greater internal volatile loss and perhaps differentiation. Fewer organic volatiles could then lead to less creation of dark organic tholins. Such a process would lead to higher albedos for these larger objects, which is indeed observed, but also bluer colors, which is not observed. An alternative explanation could invoke the satellite-forming impacts that these objects experience in an attempt to explain their surface compositions. Our understanding of the processes affecting the colors and compositions of all of the objects in the Kuiper belt is still primitive.

4.2. Satellites

The largest KBOs appear to have a different style of satellite formation than the other objects. These objects have a greater frequency of satellites, the only two known multiple satellite systems, and the possibility of much smaller satellites. Brown et al. (2006*b*) found in an adaptive optics survey of the four largest KBOs that the proba-

bility that three out of four of these would have detectable satellites suggests that they are drawn from a different population than the remainder of the Kuiper belt at the 98.2% confidence level. Updating this calculation for our currently defined population, we find that the probability that five or more out of eight in our sample of large objects are drawn from the same population as the remainder of the Kuiper belt is less than 1%.

The presence of relatively small satellites around Eris, Pluto, 2003 EL61, and Quaoar suggests formation by impact, rather than dynamical-friction aided capture. The moderate size and tight circular orbit of the satellite of Orcus could also indicate a collisional rather than capture origin. After the early discovery of near-equal brightness well-separated eccentrically-orbiting KBO binaries (see chapter by Noll et al.) much emphasis was placed on trying to explain the genesis of these unusual systems through some sort of capture mechanism. Collisions, however, appear a dominant satellite-creating process among the largest KBOs and perhaps also for the now numerous known closely spaced binaries.

4.3. Densities

The abundance of satellites and the ability to make accurate size measurements (see chapter by Stansberry et al.) allows determination of the density for many of the largest KBOs. While the handful of smaller KBOs with known densities appear to have unexpectedly low densities of $\sim 1 \text{ g cm}^{-3}$ and even lower (Stansberry et al. 2006), the largest KBOs have densities between ~ 1.9 and 2.5 g cm^{-3} as expected from cosmochemical abundances in the outer solar system (McKinnon and Mueller 1989). Figure 6 shows the measured densities of the large KBOs, including Triton and Charon. Within the largest KBOs, no statistically significant trend exists in KBO density versus radius. Similarly, no significant trend is seen in the densities of the icy satellites of the outer three planets through this size range. A rank correlation test shows that the KBOs are more dense than the icy satellites, however, at the 95% confidence level. These higher densities could be the result of the different formation environment between the proto-solar and proto-giant planet nebulae, though a bias in KBO densities caused by impacts cannot be ruled out, as density measure-

ments of KBOs (with the exception of Triton) require the presence of a satellite.

5. Conclusions

Each of the largest KBOs has a unique dynamical and physical history which can be gleaned from detailed observations such as described here. As a whole, the largest KBOs appear distinct in surface composition, satellite frequency and style, and density. Impacts appear to have played a more discernible role among the largest KBOs than among the population at large.

Based on the latitudinal completeness of the Palomar survey, it appears that 2 or 3 more KBOs of the size range of those described here likely await discovery, though many more large objects must exist in the distant regions beyond the Kuiper belt. The most likely location to find large undiscovered Kuiper belt objects is in the band at 10 degrees south ecliptic latitude where the sky densities are highest and the completeness is lowest, though with the low numbers remaining to be found they could be almost anywhere within the Kuiper belt.

Several outstanding questions remain about the largest Kuiper belt objects:

- Why are there no large KBOs among the cold classical population?
- What does Sedna's dynamical location tell us about the history of the solar system?
- What causes the density enhancements at ± 10 degrees ecliptic latitude and what implication does this have for the formation of the Kuiper belt?
- How does atmospheric cycling affect the presence and layering of species on volatile-rich large KBOs?
- Why are the water absorption features of 2003 EL61 and its satellites and fragments distinctly deeper than those of other water-rich KBOs?
- Are multiple satellite systems common among the large KBOs?
- Is Quaoar at the transition from having a volatile-rich to a volatile-poor surface?

- Are any active sources of methane, such as serpentinization of ultramafic rock, necessary to explain the volatiles on the largest KBOs?
- Is the impact frequency required to explain all of the presumably impact-related features of the large KBOs higher than expected?
- Do impacts such as those experienced by 2003 EL61 raise the densities on other KBOs?
- What explains the difference between the water ice-rich surfaces of some moderate sized KBOs and the spectrally featureless surfaces of others?

The recent discoveries of these largest KBO ensures an accessible population for addressing these questions and promises a slew of new questions as more details of these objects are discerned.

REFERENCES

- Barkume, K. M., M. E. Brown, and E. L. Schaller. 2005. Near Infrared Spectroscopy of Icy Planets. AAS/Division for Planetary Sciences Meeting Abstracts **37**:52.11.
- Barkume, K. M., M. E. Brown, and E. L. Schaller. 2006. Water Ice on the Satellite of Kuiper Belt Object 2003 EL61. *ApJ***640**:L87–L89.
- Barucci, M. A., D. P. Cruikshank, E. Dotto, F. Merlin, F. Poulet, C. Dalle Ore, S. Fornasier, and C. de Bergh. 2005. Is Sedna another Triton? *A&A***439**:L1–L4.
- Bernstein, G. M., D. E. Trilling, R. L. Allen, M. E. Brown, M. Holman, and R. Malhotra. 2004. The Size Distribution of Trans-Neptunian Bodies. *AJ***128**:1364–1390.
- Bertoldi, F., W. Altenhoff, A. Weiss, K. M. Menten, and C. Thum. 2006. The trans-neptunian object UB313 is larger than Pluto. *Nature***439**:563–564.
- Brasser, R., M. J. Duncan, and H. F. Levison. 2006. Embedded star clusters and the formation of the Oort Cloud. *Icarus* **184**:59–82.

- Brown, M. E. 2002. Pluto and Charon: Formation, Seasons, Composition. *Annual Review of Earth and Planetary Sciences* **30**:307–345.
- Brown, M. E., K. M. Barkume, G. A. Blake, E. L. Schaller, D. L. Rabinowitz, H. G. Roe, and C. A. Trujillo. 2007*a*. Methane and Ethane on the Bright Kuiper Belt Object 2005 FY9. *AJ***133**:284–289.
- Brown, M. E., K. M. Barkume, D. Ragozzine, and E. L. Schaller. 2007*b*. Discovery of an Icy Collisional Family in the Kuiper Belt. *Nature*, in press .
- Brown, M. E., A. H. Bouchez, D. Rabinowitz, R. Sari, C. A. Trujillo, M. van Dam, R. Campbell, J. Chin, S. Hartman, E. Johansson, R. Lafon, D. Le Mignant, P. Stomski, D. Summers, and P. Wizinowich. 2005*a*. Keck Observatory Laser Guide Star Adaptive Optics Discovery and Characterization of a Satellite to the Large Kuiper Belt Object 2003 EL61. *ApJ***632**:L45–L48.
- Brown, M. E., and W. M. Calvin. 2000. Evidence for Crystalline Water and Ammonia Ices on Pluto’s Satellite Charon. *Science* **287**:107–109.
- Brown, M. E., and E. L. Schaller. 2007. The mass of dwarf planet Eris. submitted.
- Brown, M. E., E. L. Schaller, H. G. Roe, D. L. Rabinowitz, and C. A. Trujillo. 2006*a*. Direct Measurement of the Size of 2003 UB313 from the Hubble Space Telescope. *ApJ***643**:L61–L63.
- Brown, M. E., and T.-A. Suer. 2007. Small satellites of big Kuiper belt objects. *AJ*, submitted.
- Brown, M. E., C. Trujillo, and D. Rabinowitz. 2004. Discovery of a Candidate Inner Oort Cloud Planetoid. *ApJ***617**:645–649.
- Brown, M. E., C. A. Trujillo, and D. L. Rabinowitz. 2005*b*. Discovery of a Planetary-sized Object in the Scattered Kuiper Belt. *ApJ***635**:L97–L100.
- Brown, M. E., M. A. van Dam, A. H. Bouchez, D. Le Mignant, R. D. Campbell, J. C. Y. Chin, A. Conrad, S. K. Hartman, E. M. Johansson, R. E. Lafon, D. L. Rabinowitz, P. J. Stomski, Jr., D. M. Summers, C. A. Trujillo, and P. L. Wizinowich. 2006*b*. Satellites of the Largest Kuiper Belt Objects. *ApJ***639**:L43–L46.
- Buie, M. W., W. M. Grundy, E. F. Young, L. A. Young, and S. A. Stern. 2006. Orbits and Photometry of Pluto’s Satellites: Charon, S/2005 P1, and S/2005 P2. *AJ***132**:290–298.
- Canup, R. M. 2005. A Giant Impact Origin of Pluto-Charon. *Science* **307**:546–550.
- Carraro, G., M. Maris, D. Bertin, and M. G. Parisi. 2006. Time series photometry of the dwarf planet ERIS (2003 UB313). *A&A***460**:L39–L42.
- Christy, J. W., and R. S. Harrington. 1978. The satellite of Pluto. *AJ***83**:1005–+.
- de Bergh, C., A. Delsanti, G. P. Tozzi, E. Dotto, A. Doressoundiram, and M. A. Barucci. 2005. The surface of the transneptunian object 90482 Orcus. *A&A***437**:1115–1120.
- Gladman, B., and C. Chan. 2006. Production of the Extended Scattered Disk by Rogue Planets. *ApJ***643**:L135–L138.
- Goldreich, P., Y. Lithwick, and R. Sari. 2002. Formation of Kuiper-belt binaries by dynamical friction and three-body encounters. *Nature***420**:643–646.
- Gomes, R. 2003. The Common Origin of the High Inclination TNO’s. *Earth Moon and Planets* **92**:29–42.
- Gomes, R. S., J. J. Matese, and J. J. Lissauer. 2006. A distant planetary-mass solar companion may have produced distant detached objects. *Icarus* **184**:589–601.
- Grundy, W. M., B. Schmitt, and E. Quirico. 1993. The Temperature-Dependent Spectra of α and β Nitrogen Ice with Application to Triton. *Icarus* **105**:254–258.
- Jewitt, D. C., and J. Luu. 2004. Crystalline water ice on the Kuiper belt object (50000) Quaoar. *Nature***432**:731–733.
- Jewitt, D. C., and S. S. Sheppard. 2002. Physical Properties of Trans-Neptunian Object (20000) Varuna. *AJ***123**:2110–2120.

- Kenyon, S. J., and B. C. Bromley. 2004. Stellar encounters as the origin of distant Solar System objects in highly eccentric orbits. *Nature***432**:598–602.
- Levison, H. F., and S. A. Stern. 2001. On the Size Dependence of the Inclination Distribution of the Main Kuiper Belt. *AJ***121**:1730–1735.
- Licandro, J., W. M. Grundy, N. Pinilla-Alonso, and P. Leisy. 2006*a*. Visible spectroscopy of 2003 UB313: evidence for N₂ ice on the surface of the largest TNO? *A&A***458**:L5–L8.
- Licandro, J., N. Pinilla-Alonso, M. Pedani, E. Oliva, G. P. Tozzi, and W. M. Grundy. 2006*b*. The methane ice rich surface of large TNO 2005 FY9: a Pluto-twin in the trans-neptunian belt? *A&A***445**:L35–L38.
- McKinnon, W. B., and S. Mueller. 1989. The density of Triton - A prediction. *Geophys. Res. Lett.***16**:591–594.
- Morbidelli, A., and M. E. Brown. 2005. Comets II, ed. M.C. Festou, H.U. Keller, H.A. Weaver (U. Arizona Press: 2005).
- Morbidelli, A., and H. F. Levison. 2004. Scenarios for the Origin of the Orbits of the Trans-Neptunian Objects 2000 CR105 and 2003 VB12 (Sedna). *AJ***128**:2564–2576.
- Rabinowitz, D. L., K. Barkume, M. E. Brown, H. Roe, M. Schwartz, S. Tourtellotte, and C. Trujillo. 2006. Photometric Observations Constraining the Size, Shape, and Albedo of 2003 EL61, a Rapidly Rotating, Pluto-sized Object in the Kuiper Belt. *ApJ***639**:1238–1251.
- Schaller, E. L., and M. E. Brown. 2007. Volatile Loss and Retention on Kuiper Belt Objects. *ApJ*, in press .
- Stansberry, J. A., W. M. Grundy, J. L. Margot, D. P. Cruikshank, J. P. Emery, G. H. Rieke, and D. E. Trilling. 2006. The Albedo, Size, and Density of Binary Kuiper Belt Object (47171) 1999 TC36. *ApJ***643**:556–566.
- Tegler, S. C., W. M. Grundy, W. Romanishin, G. J. Consolmagno, K. Mogren, and F. Vilas. 2007. Optical Spectroscopy of the Large Kuiper Belt Objects 136472 (2005 FY9) and 136108 (2003 EL61). *AJ***133**:526–530.
- Trujillo, C. A., and M. E. Brown. 2003. The Caltech Wide Area Sky Survey. *Earth Moon and Planets* **92**:99–112.
- Trujillo, C. A., M. E. Brown, K. M. Barkume, E. L. Schaller, and D. L. Rabinowitz. 2007. The Surface of 2003 EL₆₁ in the Near-Infrared. *ApJ***655**:1172–1178.
- Trujillo, C. A., M. E. Brown, D. L. Rabinowitz, and T. R. Geballe. 2005. Near-Infrared Surface Properties of the Two Intrinsically Brightest Minor Planets: (90377) Sedna and (90482) Orcus. *ApJ***627**:1057–1065.
- Tryka, K. A., R. H. Brown, and V. Anicich. 1995. Near-infrared absorption coefficients of solid nitrogen as a function of temperature. *Icarus* **116**:409–414.
- Weaver, H. A., S. A. Stern, M. J. Mutchler, A. J. Steffl, M. W. Buie, W. J. Merline, J. R. Spencer, E. F. Young, and L. A. Young. 2006. Discovery of two new satellites of Pluto. *Nature***439**:943–945.
- Young, E. F., R. P. Binzel, and K. Crane. 2001. A Two-Color Map of Pluto’s Sub-Charon Hemisphere. *AJ***121**:552–561.

This 2-column preprint was prepared with the AAS L^AT_EX macros v5.0.

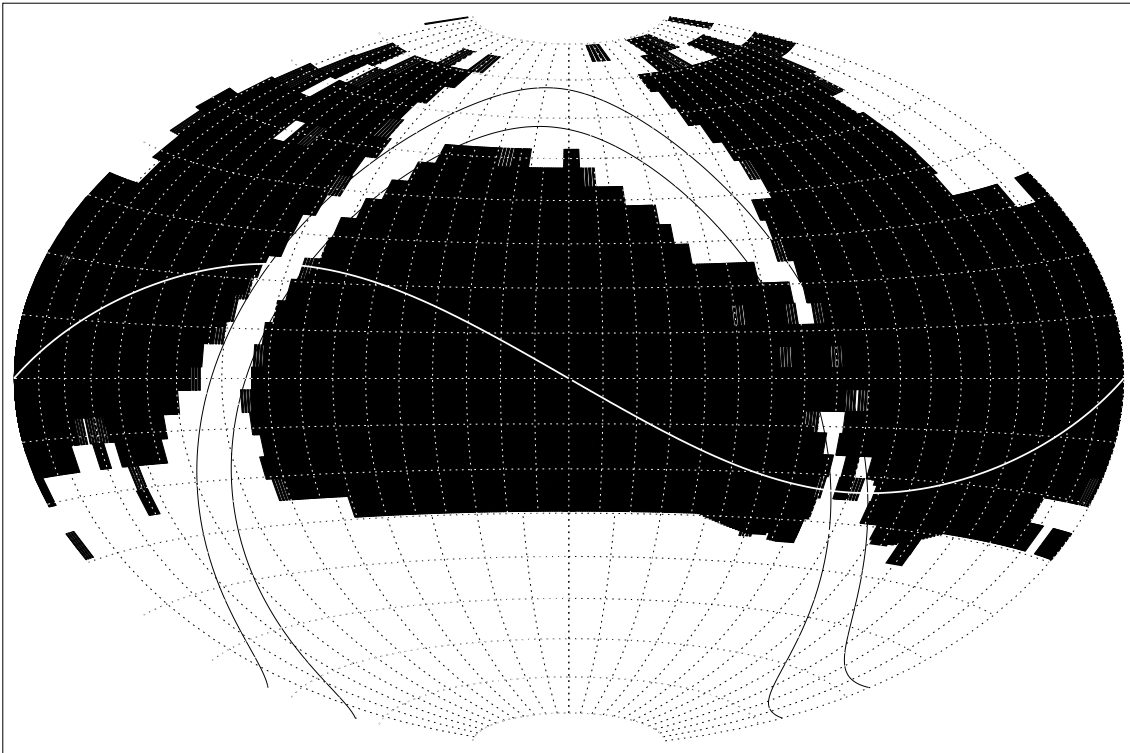


Fig. 1.— Coverage of the Palomar survey for large Kuiper belt objects. The map is centered at RA and declination of 0 degrees. The white line shows the ecliptic. Approximately 20,000 square degrees north of -30 degrees declination, mostly avoiding the galactic plane, have been covered to a limiting magnitude of $R \sim 20.5$. 71 large KBOs have been found in the survey, including most of the large KBOs discussed here.

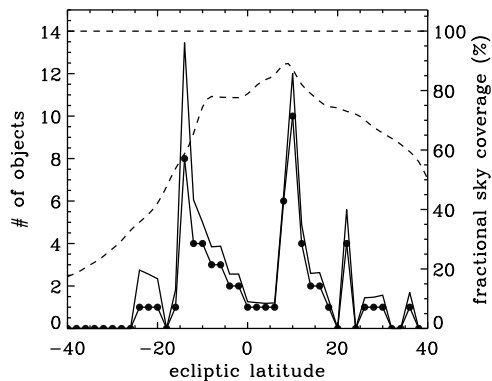


Fig. 2.— The latitudinal distribution of objects found in the Palomar survey for large KBOs. The lower line with dots shows the number of KBO detections in two degree bins. The dashed line shows the fractional sky coverage as a function of ecliptic latitude. Sky coverage is incomplete because of galactic plane avoidance, (substantial) gaps between CCDs in the mosaic camera, and occasional lack of sky coverage. The solid line above the dots shows the expected number of large KBOs per latitude bin corrected for sky coverage. The prominent peaks in sky density at -10 and $+10$ ecliptic latitude are likely a general property of the high inclination Kuiper belt rather than a property of only the large KBOs.

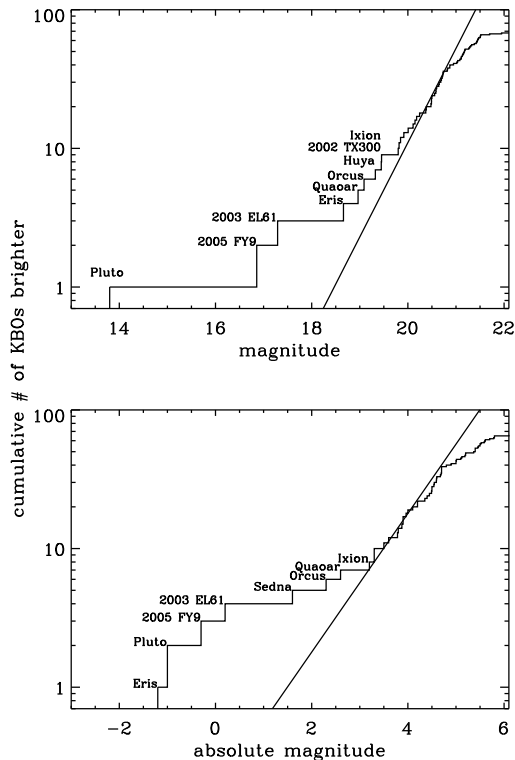


Fig. 3.— The cumulative magnitude distribution of the large KBOs found in the Palomar survey. The upper plot shows the total number of KBOs detected brighter than a limiting R magnitude, while the straight line shows the slope of the Bernstein et al. (2004) power law fit to the distribution of the excited population. The deviation from the power law at magnitudes fainter than ~ 20.5 is an indication of where the survey begins to become incomplete. The deviation from the power law for the brightest objects, also seen in the distribution of absolute magnitude in the lower plot, is an indication of the increase in albedo of the largest objects.

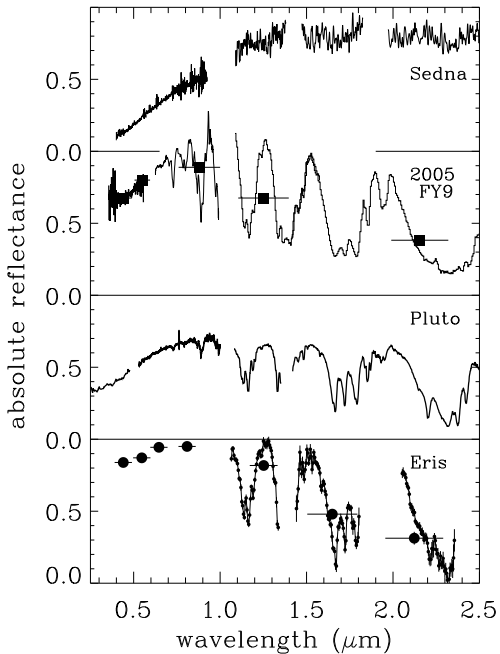


Fig. 4.— Visible-to-infrared spectra of the four methane-covered objects (Barucci et al. 2005; Brown et al. 2007a; Brown 2002; Brown et al. 2005b). While each of the objects is dominated by the signature of methane (with the exception of Sedna where the signal is weak but convincing), major differences appear in the objects’ surface compositions. Methane on Eris and 2005 FY9 appears to be dominantly in pure form, while on Pluto much of the methane is dissolved in N_2 , whose spectral signature can be seen at $2.15 \mu\text{m}$. On 2005 FY9, large path lengths through pure methane give rise to broad saturated bands, and absorption due to ethane can be seen at what should be the flat bottom of the $2.3 \mu\text{m}$ methane absorption. The low signal-to-noise of the Sedna spectra prevents detailed analysis, but the weakness of the methane and the possible presence of a broad N_2 line show a different surface character.

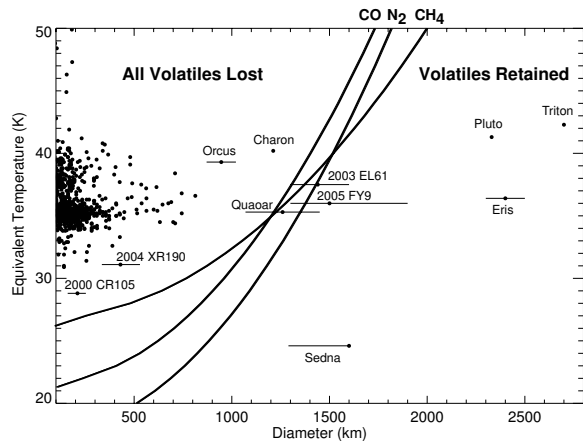


Fig. 5.— A model of surface volatile loss on objects in the Kuiper belt (Schaller and Brown, 2007). Most objects in the Kuiper belt are sufficiently small or sufficiently hot that atmospheric loss will remove all accessible surface volatiles over the lifetime of the solar system. No volatiles have been detected on any of these objects. A small number of objects are large enough or cold enough to easily retain surface volatiles, and each of these has indeed had surface volatiles detected. Three objects are in the transition region between certain volatile loss and possible volatile retention. 2003 EL61 has no volatiles detected on the surface, but the mantle shattering impact that it likely experienced would likely have removed many of the volatiles along with much of the water ice. 2005 FY9 indeed appears to be a transition object as the model predicts, with methane clearly present, but a large depletion of nitrogen relative to methane. Quaoar has a dominantly water ice spectra, but an absorption feature at $2.2 \mu\text{m}$ could be interpreted as being due to the strongest band of methane being weakly present, implying that Quaoar, too, is currently undergoing the transition from a volatile-rich to volatile-poor surface.

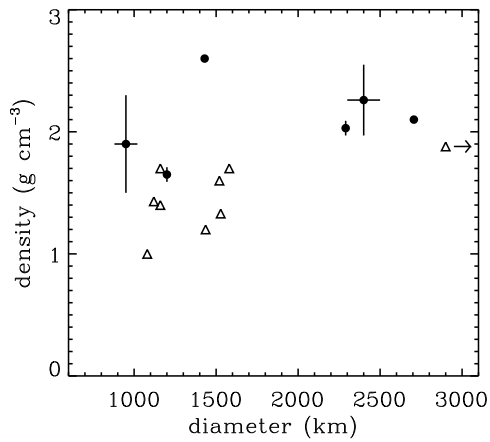


Fig. 6.— Densities of the largest KBOs, shown with solid circles. No clear trend exists in density with size, though several KBOs with smaller sizes are known to have significantly lower densities. No statistically significant trend is seen among the densities of icy satellite of the outer three planets over this same size range (open triangles; the triangle with an arrow represents Titan, with a diameter of 5150 km). The KBOs are more dense than the satellites at the 95% confidence level.

TABLE 1
 PROPERTIES OF THE LARGEST KUIPER BELT OBJECTS

	Eris	Pluto	2005 FY9	2003 EL61	Sedna	Quaoar	Orcus	Ixion
diameter (km)	2400±100	2290	1500±300	~2000 x 1500 x 1000	1300-1800	1260±190	950±70	590±190
a (AU)	67.8	39.6	45.7	43.2	488	43.1	39.4	39.3
e	0.44	0.25	0.15	0.19	0.84	0.04	0.22	0.25
i (deg)	44.0	17.1	29.0	28.2	11.9	8.00	20.5	19.7
r (AU)	96.8	31.2	52.0	51.1	88.5	43.3	47.8	42.1
H	-1.2	-1.0	-0.3	0.3	1.6	2.7	2.3	3.4
surface composition	CH ₄ +?	CH ₄ +CO+N ₂	CH ₄ +C ₂ H ₆	H ₂ O	CH ₄ +N ₂	H ₂ O + ?	H ₂ O	?
albedo (%)	86±7	50-65	80 ⁺¹⁰ ₋₂₀	~73	15-30	9±3	20±3	15 ⁺¹⁵ ₋₆
mass (10 ²⁰ kg)	166±2	130.5±0.6	-	42±1	-	-	9±1	-
density (g cm ⁻³)	2.3±0.3	2.03±0.06	-	~2.6	-	-	1.9±0.4	-
satellite frac. brightness (%)	0.4	18,.018,.015	-	5.9,1.5	-	0.6	8	-
satellite period (days)	15.8	6.4,38.2,24.8	-	49.1,?	-	?	9.8	-
additional sat. limit (%)	0.04	0.001	0.01	0.5	0.2	0.2	0.1	0.5

NOTE.—References for all data can be found throughout the text.